International Journal on Artificial Intelligence Tools
Vol. 12, No. 1 (2003) 1–16

World Scientific
www.worldscientific.com

ODOR MIXTURES AND CHEMOSENSORY ADAPTATION IN GAS SENSOR ARRAYS

RICARDO GUTIERREZ-OSUNA*
Department of Computer Science
Texas A&M University
College Station, TX 77843

NILESH U. POWAR
Department of Computer Science and Engineering
Wright State University
Dayton, OH 45435

Received 8 April 2002
Accepted 3 January 2003

Inspired by the process of olfactory adaptation in biological olfactory systems, this article presents two algorithms that allow a chemical sensor array to reduce its sensitivity to odors previously detected in the environment. The first algorithm is based on a committee machine of linear discriminant functions that operate on multiple subsets of the overall sensory input. Adaptation occurs by depressing the voting strength of discriminant functions that display higher sensitivity to previously detected odors. The second algorithm is based on a topology-preserving linear projection derived from Fisher's class separability criteria. In this case, the process of adaptation is implemented through a reformulation of the between-to-within-class scatter eigenvalue problem. The proposed algorithms are validated on two datasets of binary and ternary mixtures of organic solvents using an array of temperature-modulated metal-oxide chemoresistors.

Keywords: Gas sensor arrays; chemosensory adaptation; machine olfaction; committee machines; linear discriminant analysis

1. Introduction

The integration of gas sensor arrays and pattern analysis algorithms has received much attention in recent years as a low-cost alternative to odor measurement, conventionally carried out with analytical instruments or human panels [1]. The broad and overlapping selectivity of gas sensors can be exploited to characterize a wide range of odors by processing the multivariate response of a sensor array with pattern recognition algorithms. A number of chemical analysis applications have appeared in the sensor-array community, ranging from classification of odors to prediction of organoleptic properties. However, despite the rapid growth in the field of machine olfaction, no publications have addressed, to the best of our knowledge, the issue of chemosensory adaptation in gas sensor

* Corresponding author (rgutier@cs.tamu.edu)

arrays. Adaptation is the mechanism by which sensory systems reduce their sensitivity to previously detected stimuli, preventing sensory overflow in the central nervous system and improving the ability to detect new stimuli [2]. For instance, a person entering a coffee shop will be immediately overwhelmed by the smell of fresh ground coffee, but that sensation will automatically fade away until it is no longer noticed.

The purpose of this paper is to investigate computational mechanisms that allow a gas sensor array to mimic certain aspects of the adaptation process. In particular, we focus on the perception of odor mixtures under adaptation to one of the mixture components, a scenario where the organism shifts the perceived quality towards the remaining component(s) in the mixture [3, 4].

2. The Olfactory Pathway

We briefly review the mammalian olfactory pathway, from which two key signal-processing elements are borrowed for this work: (*i*) the role of glomeruli as functional units and (*ii*) the modulation of bulbar activity through centrifugal feedback. As illustrated in Fig. 1, the olfactory pathway can be divided into three basic subsystems: olfactory epithelium, olfactory bulb and olfactory cortex [5, 6]. Volatile compounds entering the nostrils are detected in the olfactory epithelium by a large number (10-100 million) of olfactory neurons. The pioneering work of Buck and Axel [7] has lead to the identification of a family of approximately 1,000 receptor proteins that are responsible for this molecular detection process. Each olfactory neuron appears to be dedicated to a particular receptor [8], but each receptor can identify multiple odorants, and each odorant can be identified by multiple receptors [9], leading to a combinatorial coding of odors.

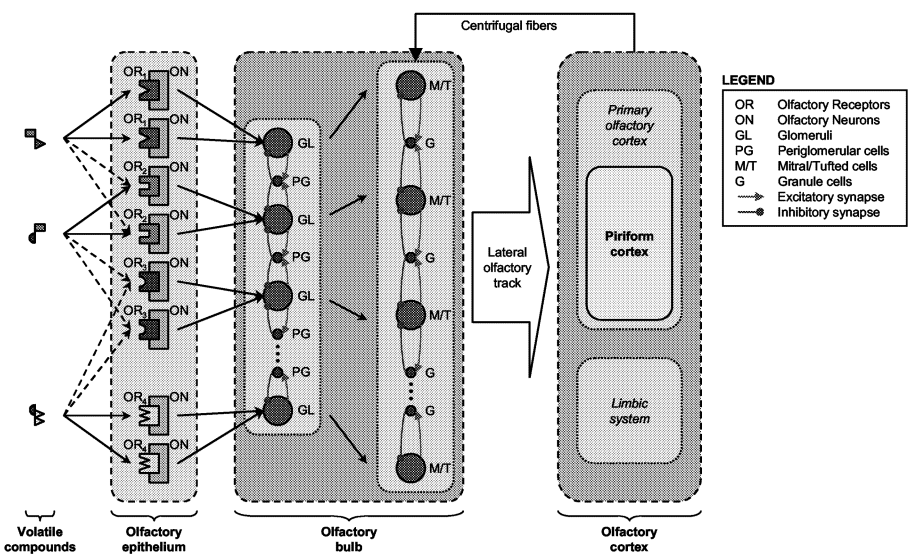

Fig. 1. Computational model of the olfactory pathway (adapted from [6, 9]).

Bundles of olfactory neuron axons access the brain via the cribiform plate, relaying their information to mitral and tufted cells in the olfactory bulb through spherical clusters of synapses called glomeruli. Nearly 25,000 receptor axons converge to each glomerulus,

which in turn connects to approximately 25 mitral cells and 70 tufted cells. A close look at the olfactory bulb reveals a number of local microcircuits, mediated by periglomerular and granule cells, which perform complex excitatory and inhibitory functions at the glomerular and mitral/tufted levels, respectively [10, 11, 12]. Of particular interest to our work is the fact that neurons expressing the same receptor appear to converge onto single or a small subset of glomeruli in the olfactory bulb [8], supporting a fifty-year-old hypothesis according to which glomeruli serve as functional units or "labeled lines" for a subset of odorant molecules [cf. 10 and references therein]. Additional evidence indicates that odor quality may be encoded by spatial patterns in the olfactory epithelium and the glomerular layer [13, 14], whereas odor intensity would be encoded by the number of active receptors [15].

Mitral/tufted cell axons form the lateral olfactory tract, which transmits olfactory information to the olfactory cortex. The main target of the lateral olfactory tract is a collection of cortical regions collectively called the primary olfactory cortex. Among those regions, the piriform cortex is the largest area and plays a central role in the conscious recognition of odors. In addition, the lateral olfactory tract is heavily interconnected with the limbic system, which explains the effects of smell on emotions and mood. Finally, the olfactory cortex sends centrifugal inputs back to the olfactory bulb (primarily to the granule layer), resulting in a complex feedback mechanism that is believed to play a central role in odor segmentation and adaptation [4, 16].

3. Chemosensory Adaptation with Committee Machines

As mentioned in the previous section, the convergence of neurons expressing the same receptor onto a single or a small set of glomeruli substantiates the hypothesis that glomeruli serve as functional units that flag the presence of specific odors in the environment. In accordance with this view, we propose the classification architecture depicted in Fig. 2. Sensory inputs with similar selectivity profiles form bundles $s^{(k}$ that act as feature subsets for a family of discriminant functions $g_c^{(k}$:

$$g_c^{(k}\left(s^{(k}\right)=\begin{cases}1 & s\in\omega_c\\ -1 & s\notin\omega_c\end{cases} \tag{1}$$

where the activation level of each discriminant $g_c^{(k}$ indicates the presence (or absence) of odor ω_c. In this work, we model each of these discriminants as a multi-linear regression function $g_c^{(k}\left(s^{(k}\right)=G_c^{(k}s^{(k}+H_c^{(k}$, whose parameters are estimated through least-squares minimization:

$$\left[G_c^{(k},H_c^{(k}\right]=\arg\min_{G,H}\left[\sum_{\forall s^{(k}}\left(Gs^{(k}+H-g_c^{(k}\left(s^{(k}\right)\right)^2\right] \tag{2}$$

Activation levels from these discriminants are passed to a higher processing layer where they are combined into a cumulative discriminant function $g_c(s)$ using a committee machine with a weighted ensemble average [17]:

$$g_c(s)=\frac{\sum_k f\left(g_c^{(k}\left(s^{(k}\right)\right)w_c^{(k}\left(1-i^{(k}\right)}{\sum_k w_c^{(k}} \tag{3}$$

where $s=[s^{(1},s^{(2},s^{(3},...]$ is the overall sensory input, $w_c^{(k}$ is a weighting coefficient that measures the selectivity of sensory bundle $s^{(k}$ to odor class ω_c, and $i^{(k}$ is an inhibitory term to excite/depress the contribution of $s^{(k}$. The term $\sum_k w_c^{(k}$ in the denominator is used to normalize the response relative to the overall sensitivity of the sensor array to each odor. Finally, the transform $f(\cdot)$ is a squashing sigmoidal function that limits the activation level of the discriminant functions in the range [0,1]:

$$f(x)=\frac{1}{2}(\tanh(x)+1) \tag{4}$$

The use of the selectivity coefficients $w_c^{(k}$ in the ensemble average (3) allows the committee machine to weight the contribution of each discriminant function $g_c^{(k}$ according to its specificity for odor class ω_c. These selectivity coefficients are estimated as the average activation level of $g_c^{(k}$ to input s_{c^+}, where the term c^+ indicates that the input is a mixture containing odor ω_c *plus* others:

$$w_c^{(k}=E\left[g_c^{(k}\left(s_{c^+}^{(k}\right)\right]_{\forall c^+} \tag{5}$$

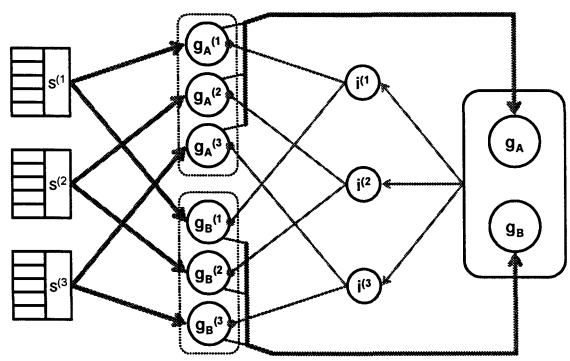

Fig. 2. Structure of the committee machine with sensory bundles $s^{(k}$, discriminant functions $g_c^{(k}$, cumulative discriminants g_c and inhibitory feedback $i^{(k}$.

Adaptation in this model is achieved by means of the inhibitory terms $i^{(k}$, which feed back the activation level of the cumulative discriminant $g_c(s)$ to previous stimuli, properly scaled and normalized by the selectivity coefficients $w_c^{(k}$:

$$i^{(k}(s)=\tanh\left(\lambda\frac{\sum_c g_c(s)w_c^{(k}}{\sum_c w_c^{(k}}\right) \tag{6}$$

As a result of this inhibitory feedback, the contribution of each sensor bundle $s^{(k}$ is suppressed according to its sensitivity to odor ω_c, weighted by the cumulative evidence that odor ω_c was already detected in the environment. A scaling coefficient λ can be used to drive the inhibitory terms to saturation, allowing the feedback loop to operate as an ON/OFF feature selection mechanism.

3.1. *Simulating receptor bundles*

To empirically validate the proposed adaptation mechanism, we employ an array with four metal-oxide (MOX) sensors, a widely used technology in machine olfaction applications [1]. The transduction mechanism of MOX sensors is based on resistivity changes. In the presence of volatile organic compounds, oxygen ions on the surface of the sensor undergo a chemical reaction. As a result, the concentration of free electrons increases, which reduces the potential barrier between metal-oxide grain boundaries and, therefore, the electrical resistance of the material. These changes in resistance can then be measured with conventional voltage divider or Wheatstone-bridge circuits [18].

In order to increase the rate of these reactions, MOX sensors are driven at high operating temperatures (300-500°C) by applying a given voltage to a resistive heater embedded in the device. The conventional excitation mode for MOX sensors consists of applying a constant voltage to the heater, which yields an approximately constant operating temperature. The final selectivity of the device will depend on this operating temperature, since the reaction rates for different volatile compounds and the stability of adsorbed oxygen species are a function of surface temperature [19]. This temperature-selectivity dependence is commonly exploited to extract additional information by modulating the operating temperature during exposure to volatile compounds and extracting features from the dynamic response of the sensor at multiple temperatures [20]. Considering that sensor responses at similar temperatures have related selectivities, these temperature-modulated features can therefore be clustered into sensor bundles $s^{(k}$ according to the operating temperature at which they are obtained.

In a previous article [21] we have reported significant selectivity enhancements on temperature-modulated MOX sensors. The sensors were driven with a low frequency (0.125Hz-4Hz) sinusoidal heater voltage of 0-7V amplitude. It was concluded that, due to thermal inertia, lower excitation frequencies were necessary to resolve dynamic information at multiple temperatures. In this article we extend the previous approach by exciting the sensors at various temperature ranges using the heater-voltage profile shown in Fig. 3. This profile contains six sinusoidal segments with a 1-6V DC offset in increments of 1V. Each segment consists of five sinusoidal cycles with an amplitude of 2V and a period of T=20s. In order to eliminate thermal transients associated with each step in DC offset, only the last cycle of each segment is used for pattern analysis [22]. The dynamic trajectory of the sensor at each temperature range is captured by sub-sampling the last cycle down to 10 samples, as depicted in the inset of Fig. 3, which results in a 10-dimensional feature vector for each temperature range. Each of these feature vectors can then be associated with a bundle of "receptors" having similar selectivity profiles. Given that the array consists of four sensors excited at six temperature ranges, our procedure yields twenty-four 10-dimensional feature vectors (or bundles $s^{(k}$), which are used to obtain the corresponding linear discriminant functions $g_c^{(k}$ (k = 1-24) for each analyte.

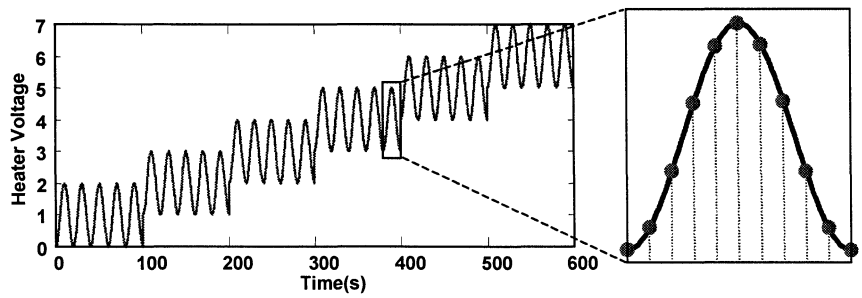

Fig. 3. Heater voltage profile for the MOX sensors (left) and bundles of temperature-modulated features (right).

3.2. *Experimental*

The aforementioned temperature modulation approach was used to collect an experimental dataset on an array of four Figaro sensors (2602, 2610, 2611, 2620) [23]. The sensors were mounted on the cap of a 30 ml vial containing 10 ml of analytes. Acetone (odor *A*), ethanol (odor *B*) and a 50/50 mixture of these two analytes were employed as analytes. The resistance of the sensors was measured at 10 samples/second using voltage dividers connected to a LabVIEW-driven data acquisition card. Fifteen samples per odor were collected over a period of five days. The average response of the four sensors vs. the cyclic heater voltage is shown in Fig. 4. Only the fifth cycle of each segment is plotted. It can be observed that, although the sensors have overlapping selectivities, they respond differently to the analytes at the various temperature ranges. Notice the unique pattern of sensor 4 in the 5-7V, which clearly discriminates acetone from ethanol. Of particular significance is the behavior of the 50/50 mixture on the different sensors and temperature ranges: the mixture generates a pattern similar to acetone on sensor 1 (practically identical on the 3-5V range) but similar to ethanol on the other three sensors. This behavior is critical to the success of our approach because it allows the system to bias the perception of mixtures by favoring certain sensors and temperature ranges.

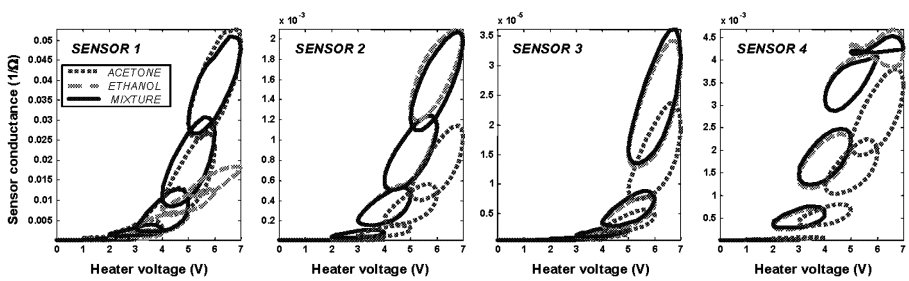

Fig. 4. Sensor conductance versus cyclic heater voltage for acetone (dotted), ethanol (dashed) and 50/50 mixture (solid).

The regression matrices $\left(G_A^{(k)}, H_A^{(k)}\right)$ are trained using pure acetone, whereas $\left(G_B^{(k)}, H_B^{(k)}\right)$ are obtained from the pure ethanol samples. The mixture samples are used to determine the selectivity coefficients $w_c^{(k)}$. The results are shown in Fig. 5, where the inhibitory

terms $i^{(k}$ have been set to zero to illustrate the performance of the system prior to adaptation. Each row denotes an example and each column a discriminant function. The first 15 rows correspond to acetone samples, the next 15 rows correspond to ethanol samples and the last 15 rows are for the 50/50 mixture. Columns 1-24 correspond to the discriminant functions for the first odor class. Columns 1-6 are associated to the response of sensor 1 at each of the six heater voltage ranges: 0-2V, 1-3V, ...5-7V, respectively. Columns 7-12 are for sensor 2, and so forth. Several conclusions can be extracted from these results. First, the linear discriminant functions can clearly identify the individual analytes: the $f\left(g_A^{(k}\right)$ block responds selectively to acetone but not to ethanol, whereas the $f\left(g_B^{(k}\right)$ block responds mostly to ethanol. Second, the response of the sensors at low temperature (0-2V, 1-3V) is not discriminative, as illustrated by the response of columns 1, 7, 8, 13, etc. Third, the discriminant functions have complementary responses to the 50/50 mixture (rows 31-45). Columns 3-6 are high and columns 27-30 are low, indicating that the corresponding discriminants would classify these samples as acetone. The reverse classification occurs with the remaining columns. All these results are consistent with the structure of the cyclic patterns in Fig. 4.

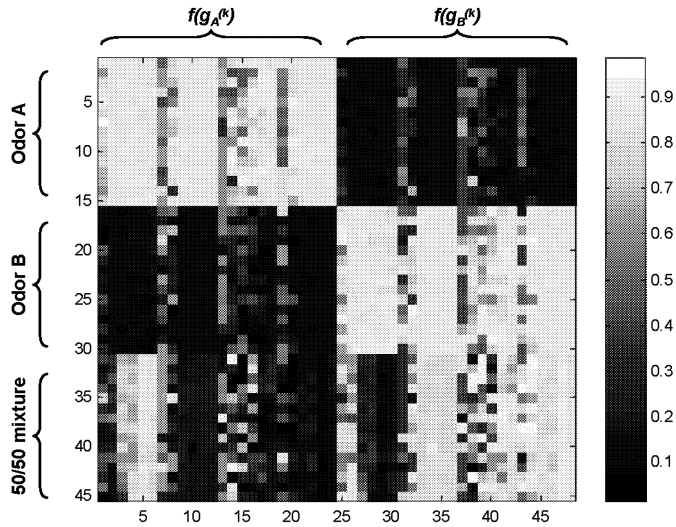

Fig. 5. Activation level of the linear discriminant functions (columns) for each odor example (rows).

We are finally ready to test the ability of the algorithm to mimic chemosensory adaptation by analyzing the activation level of the cumulative discriminant functions $g_c(s)$ after the system has identified a pure analyte and has set the inhibitory terms $i^{(k}$ accordingly. The results are illustrated in Fig. 6, where a value of $\lambda = 10$ (empirically determined) was used in equation (6). In the absence of adaptation, as shown in Fig. 6(a), each cumulative discriminant $g_c(s)$ present a high level when $s \in \omega_c$ and a low level otherwise. The 50/50 mixture induces a high activation pattern on both cumulative discriminants, although $g_B(s)$ dominates since the mixture is closer to odor B on three out

of the four sensors and, therefore, more discriminant functions $g_B^{(k}$ become activated. When the system adapts to odor A, the activation level of $g_A(s)$ drops significantly for all samples, including those from class A. As a result, the activation pattern for the 50/50 mixture becomes similar to that of odor B, as shown in Fig. 6(b). Conversely, when the system adapts to odor B, the activation level of $g_B(s)$ becomes very small, and the 50/50 mixture presents a pattern that resembles that of odor A. From the vertical scales in Fig. 6, it can also be observed that the algorithm lowers the overall activation levels on both cumulative discriminants, a cross-adaptation phenomenon caused by the high level of collinearity endemic to MOX sensors. Therefore, classification under these conditions should be performed by considering the ratio of cumulative discriminants rather than their absolute value.

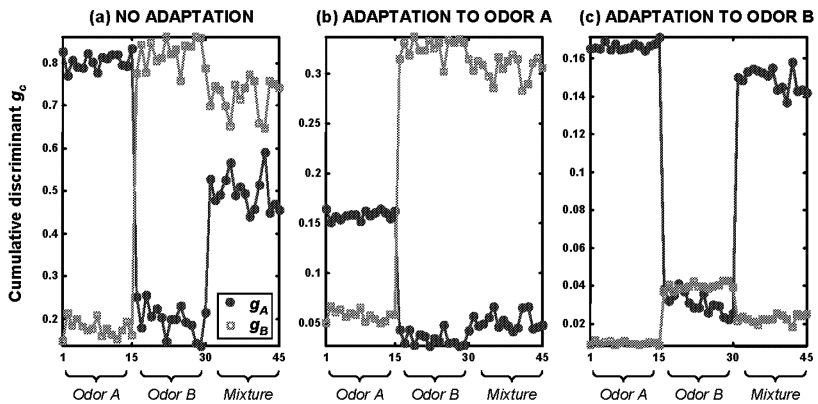

Fig. 6. Cumulative discriminant activation g_A (circles) and g_B (squares) for different adaptation scenarios. Under adaptation to an odor, the binary mixture is perceived as the second odor.

4. Chemosensory Adaptation as a Subspace Projection

The committee-machine algorithm presented in the previous section requires that the sensor bundles provide complementary information to ensure that the output of the discriminant functions to odor mixtures can account for all possible adaptation scenarios. For instance, in the example of Fig. 4 complementarity implies that the 50/50-mixture pattern should be similar to the pattern of each solvent on at least one sensor bundle. This condition is met in the binary mixture problem of the previous section, allowing the cumulative discriminants to provide a wide range of responses when exposed to a 50/50 mixture, as shown in the bottom 15 rows of Fig. 5. Clearly, as the number of analytes increases, the number of possible mixtures and adaptation scenarios grows exponentially. Unfortunately, this can pose severe limitations for chemical sensor arrays, particularly MOX sensors, which have notoriously overlapping selectivity profiles.

To address the collinearity of current commercial gas sensors, an alternative mechanism is proposed in this article. The technique, derived from Fisher's Linear Discriminant Analysis [24], facilitates the analysis of mixtures by finding a subspace projection that preserves an a-priori topology of odors. As shown in Fig. 7, each sensor bundle $s^{(k}$ (denoted by x henceforth to simplify the notation) is projected onto a lower dimensional vec-

tor y according to a linear transformation $W(c)$ that depends on a previously detected odor ω_c. In the absence of adaptation, the projection imposes a topological ordering between odors and their mixtures. When adaptation to an odor takes place, the topology is modified to generate a projection where the pattern of the adapting odor becomes closer to a background. This novel topology-preserving transform is introduced in the following subsections, and is validated on an experimental database of binary and ternary mixtures using the temperature-modulated MOX sensor array presented earlier.

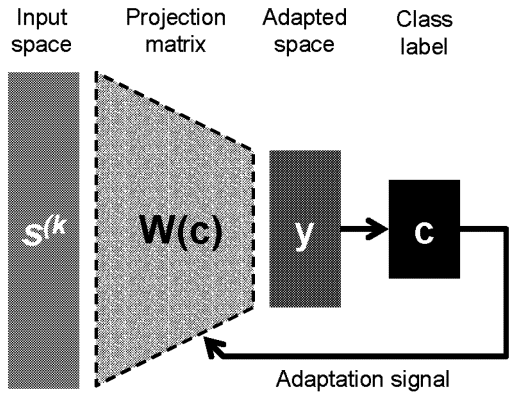

Fig. 7. Feature extraction for chemosensory adaptation. The input space $s^{(k}$ is projected onto a lower dimensional space using a projection matrix $W(c)$ that depends on previously detected odors ω_c.

4.1. *Topology-preserving Linear Discriminant Analysis (TP-LDA)*

Linear Discriminant Analysis (LDA) is a supervised dimensionality-reduction technique aimed at enhancing the discrimination of patterns in classification problems. LDA seeks a linear projection $y=Wx$ that maximizes the separation between class-conditional means while minimizing the spread of patterns within each class. It can be shown [24] that the optimal matrix W consists of the eigenvectors corresponding to the largest eigenvalues of the matrix $S_W^{-1}S_B$, where S_W and S_B are the within-class and between-class scatter matrices, respectively, defined by:

$$\mu_q = \frac{1}{n_q}\sum_{x\in\omega_q} x \quad and \quad \mu = \frac{1}{n}\sum_{\forall x} x \tag{7}$$

$$S_W = \frac{1}{n}\sum_{q=1}^{Q} S_q = \frac{1}{n}\sum_{q=1}^{Q}\sum_{x\in\omega_q}(x-\mu_q)(x-\mu_q)^T \tag{8}$$

$$S_B = \frac{1}{n}\sum_{q=1}^{Q} n_q(\mu_q-\mu)(\mu_q-\mu)^T \tag{9}$$

where Q is the number of classes, n is the total number of examples in the dataset, μ_q, S_q and n_q are the mean vector, scatter matrix and number of examples of class ω_q, respectively, and μ is the mean vector of the entire distribution. LDA generates projections that

maximize the separability of classes, but does not preserve a topological ordering of the projections, as illustrated in Fig. 8(a) for a ternary mixture problem, where single labels denote individual components and compound labels represent mixtures (e.g., AC is the 50/50 mixture of components A and C). For the purpose of mixture processing, however, it would be desirable to obtain a topological projection where the mixtures have patterns that are the average of their constituent odors, as illustrated in Fig. 8(b).

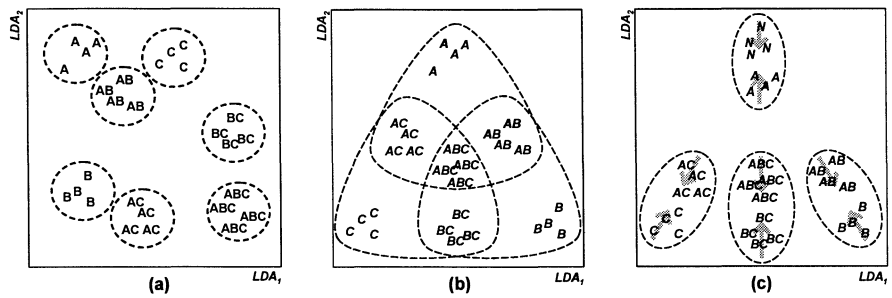

Fig. 8. Clustering of examples with LDA (a), TP-LDA (b) and TP-LDA under adaptation (c).

The conventional LDA projection shown in Fig. 8(a) is obtained by assigning separate classes to each individual component and each mixture without regard to the existing relationships (e.g., the mixture AB should be "more related" to A or B than it is to C). To ensure a topological ordering, these relationships must be taken into consideration when computing the mean vectors and scatter matrices in equations (7-9). Essentially, to ensure that examples from mixture AB project between those of A and B, the mean vectors of these two classes should be replaced by the following expressions:

$$\begin{aligned} \mu_A &\leftarrow (\mu_A + \mu_{AB})/2 \\ \mu_B &\leftarrow (\mu_B + \mu_{AB})/2 \end{aligned} \tag{10}$$

The same idea can be applied to the computation of scatter matrices and can be generalized to mixture problems with more than two components by using a binary labeling scheme that captures the relationships between classes. Formally, given a problem with P primary odors (e.g., $Q=2^P$ mixtures), each example x is labeled with a family of P indicator variables $\Gamma^N(x) = \{\gamma_p^N(x),\ p = 1..P\}$, where $\gamma_p^N(x) = 1$ if x has primary odor p as a constituent ($p \subset x$) and zero otherwise:

$$\gamma_p^N(x) = \begin{cases} 1 & p \subset x \\ 0 & p \not\subset x \end{cases} \tag{11}$$

The superscript N (for Neutral) denotes that the topology-preserving LDA projection has not (yet) undergone chemosensory adaptation. This simple labeling scheme, illustrated in Table 1 for $P=3$, implies that mean vectors and scatter matrices in equations (7-9) are computed on the following groups of odor patterns:

$$\begin{aligned} A' &= \{A,\ AB,\ AC,\ ABC\} \\ B' &= \{B,\ AB,\ BC,\ ABC\} \\ C' &= \{C,\ AC,\ BC,\ ABC\} \end{aligned} \tag{12}$$

To make explicit use of these binary indicators, the computation of means and matrices can be redefined by:

$$\mu_p^N = \frac{1}{n_p^N} \sum_{\forall x \ni \gamma_p^N(x)=1} x \quad with \; n_p^N = \sum_{\forall x \ni \gamma_p^N(x)=1} 1 \quad and \; n_{\forall p}^N = \sum_{p=1}^{P} n_p^N \tag{13}$$

$$S_W^N = \frac{1}{n_{\forall p}^N} \sum_{p=1}^{P} S_p^N = \frac{1}{n_{\forall p}} \sum_{p=1}^{P} \sum_{\forall x \ni \gamma_p^N(x)=1} \left(x - \mu_p^N\right)\left(x - \mu_p^N\right)^T \tag{14}$$

$$S_B^N = \frac{1}{n_{\forall p}^N} \sum_{p=1}^{P} n_p^N \left(\mu_p^N - \mu\right)\left(\mu_p^N - \mu\right)^T \tag{15}$$

where μ_p^N represents the mean of all the examples that have primary analyte p as one of their constituents ($\forall x \ni \gamma_p^N(x) = 1$). As a result, the new topology-preserving projections are aligned with the eigenvectors of $\left(S_W^N\right)^{-1} S_B^N$.

Table 1. Indicator variables $\Gamma^N(x)$ for TP-LDA

Class	$\gamma_A^N(x)$	$\gamma_B^N(x)$	$\gamma_C^N(x)$
x=A	1	0	0
x=B	0	1	0
x=C	0	0	1
x=AB	1	1	0
x=AC	1	0	1
x=BC	0	1	1
X=ABC	1	1	1
x=Neutral	0	0	0

To illustrate the performance of this topology-preserving LDA (TP-LDA) projection, a ternary dataset was collected following the experimental procedure outlined in sections 3.1 and 3.2. The dataset consisted of mixtures from three organic solvents: acetone (*A*), ethanol (*B*) and isopropyl alcohol (*C*). 11% dilutions in distilled water were used to reduce the recovery time of the sensors. Five samples were collected for each of the eight possible mixtures (distilled water was used as the neutral odor). The results for the conventional LDA and the proposed TP-LDA are shown in Fig. 9(a) and (b), respectively. It can be observed that TP-LDA successfully generates a projection where the different clusters are spatially organized according to the relationship between their class labels. Samples from the neutral odor (*N*) project well outside the region of interest, and are not shown in Fig. 9.

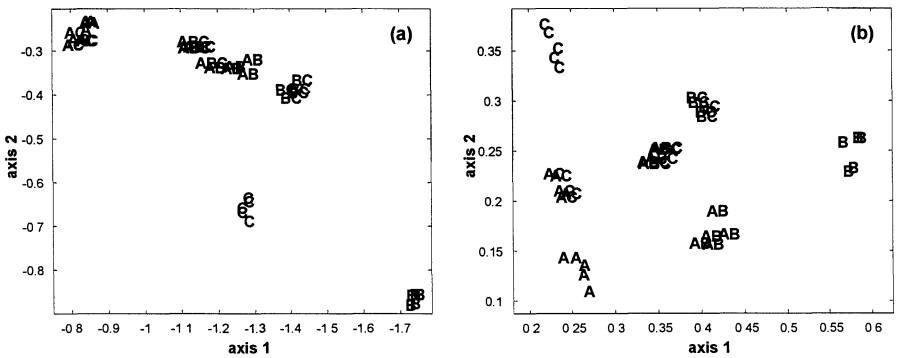

Fig. 9. Performance of LDA (a) and TP-LDA (b) on a ternary mixture database.

4.2. *Adapting the TP-LDA projection*

The proposed TP-LDA projection serves as the backbone for simulating chemosensory adaptation, since each adaptation scenario corresponds to a unique topology. Take the example of adaptation to odor A, as illustrated in Fig. 8(c). In this case, the objective of the adapted topological mapping is a projection that removes the effect of odor A on all of its mixture patterns. The mapping should therefore yield a projection where patterns from odor A overlap with those from the neutral background N, and patterns from the mixtures AB, AC and ABC overlap with those from B, C and BC, respectively. Borrowing the analogy of equation (12), such projection may be achieved by defining the following odor clusters:

$$\begin{aligned} A' &= \{A, N\} \\ B' &= \{B, AB, BC, ABC\} \\ C' &= \{C, AC, BC, ABC\} \end{aligned} \tag{16}$$

or, formally, by using a set of indicators $\Gamma^A(x) = \{\gamma_p^A(x),\ p = 1..P\}$, where superscript A denotes chemosensory adaptation to odor A. Therefore, each adapted topology can be imposed by modifying the binary indicators of the odors, which generates a different eigensolution for the problem in equations (13-15). As an example, the indicator values required for adaptation to A, B and C are shown in Table 2. In general, adaptation to a generic odor Δ (where Δ may itself be a mixture) may be achieved with the following set of indicators:

$$\gamma_p^{\Delta}(x) = \begin{cases} \gamma_p^N(x) & & p \cap \Delta = \varnothing \\ 1 & (x \cap p \neq \varnothing \ \wedge \ x \subseteq \Delta) \vee x = N & \\ 0 & \textit{otherwise} & p \cap \Delta \neq \varnothing \end{cases} \tag{17}$$

where $p \cap \Delta \neq \varnothing$ indicates that odors p and Δ have some components in common (e.g., $A \cap AB \neq \varnothing$, $C \cap AB = \varnothing$), and $x \subseteq \Delta$ indicates that all of the components in odor x are also in Δ (e.g., $A \subseteq AB$, $C \not\subset AB$). Equation (17) replaces $\gamma_p^N(x)$ when computing the mean vector and scatter matrices in equations (13-15). The resulting projections for one particular sensor bundle (TGS2620, 5-7V) for three adaptation scenarios are shown

in Fig. 10. Similar performance can be obtained on several other sensor bundles, but not on all. Notice that, in each case, the technique is able to find a projection where the adapting odor is projected close to the neutral background, and mixtures containing the adapting odor are shifted toward the other component(s). These results demonstrate the ability of the TP-LDA mapping to simulate a steady state scenario in which full adaptation has been reached. In the next subsection we present a regularization technique that allows TP-LDA to simulate the onset of the adaptation process.

Table 2. Indicator variables $\Gamma^{\Delta}(x)$ for TP-LDA under adaptation

	(a) Adaptation to A			(b) Adaptation to B			(c) Adaptation to C		
Odor class	γ_A^A	γ_B^A	γ_C^A	γ_A^B	γ_B^B	γ_C^B	γ_A^C	γ_B^C	γ_C^C
A	1	0	0	1	0	0	1	0	0
B	0	1	0	0	1	0	0	1	0
C	0	0	1	0	0	1	0	0	1
AB	0	1	0	1	0	0	1	1	0
AC	0	0	1	1	0	1	1	0	0
BC	0	1	1	0	0	1	0	1	0
ABC	0	1	1	1	0	1	1	1	0
Neutral	1	0	0	0	1	0	0	0	1

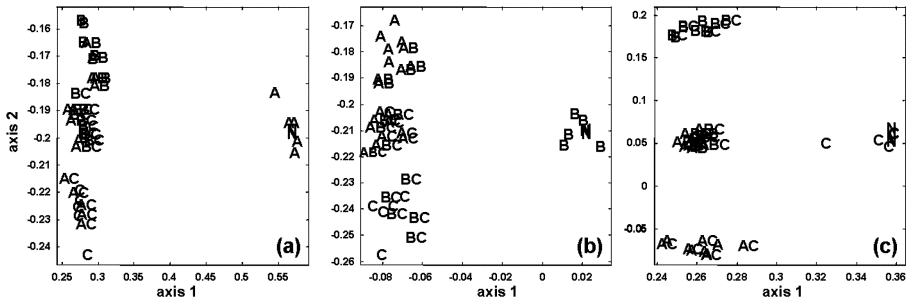

Fig. 10. Full chemosensory adaptation to odor A (a), odor B (b) and odor C (c).

4.3. *Regularizing the TP-LDA projection*

A further generalization of the TP-LDA mapping allows us to simulate partial chemosensory adaptation. We define an adaptation term η_{Δ} ($0 \le \eta_{\Delta} \le 1$, $\Delta = 1..P$) to represent the degree of adaptation to an odor, where $\eta_{\Delta}=0$ indicates that no adaptation has occurred and $\eta_{\Delta}=1$ indicates that full adaptation has been reached. This adaptation term can be used as a regularization parameter to obtain intermediate solutions between those imposed by equations (11) and (17):

$$\hat{S}_W = S_W^N \prod_{\Delta=1}^{P} (1-\eta_{\Delta}) + \sum_{\Delta=1}^{P} S_W^{\Delta} \eta_{\Delta} \tag{18}$$

$$\hat{S}_B = S_B^N \prod_{\Delta=1}^{P}(1-\eta_\Delta) + \sum_{\Delta=1}^{P} S_B^\Delta \eta_\Delta \tag{19}$$

In the absence of adaptation ($\eta_\Delta = 0 \ \forall\Delta$), these scatter matrices are identical to the non-adapted solution (S_B^N, S_W^N). In the onset of adaptation to odor Δ ($\eta_\Delta > 0$, $\eta_p = 0 \ \forall p \neq \Delta$), the solution undergoes regularization with (S_B^Δ, S_W^Δ), slowly departing from (S_B^N, S_W^N) as the adaptation parameter η_Δ grows, until full adaptation is reached and the solution becomes equivalent to (S_B^Δ, S_W^Δ). This essentially provides a smooth transition between the mappings in Fig. 9(b) and Fig. 10(a-c). The results of this regularization process are illustrated in Fig. 11 for various degrees of adaptation to odor A $\eta_A = \{0.05, 0.35, 0.65, 0.95\}$. Notice how effectively does the regularization process provide a smooth trajectory from the onset of adaptation (a) until full adaptation is achieved (d). Similar results can also be obtained when adapting to odors B and C.

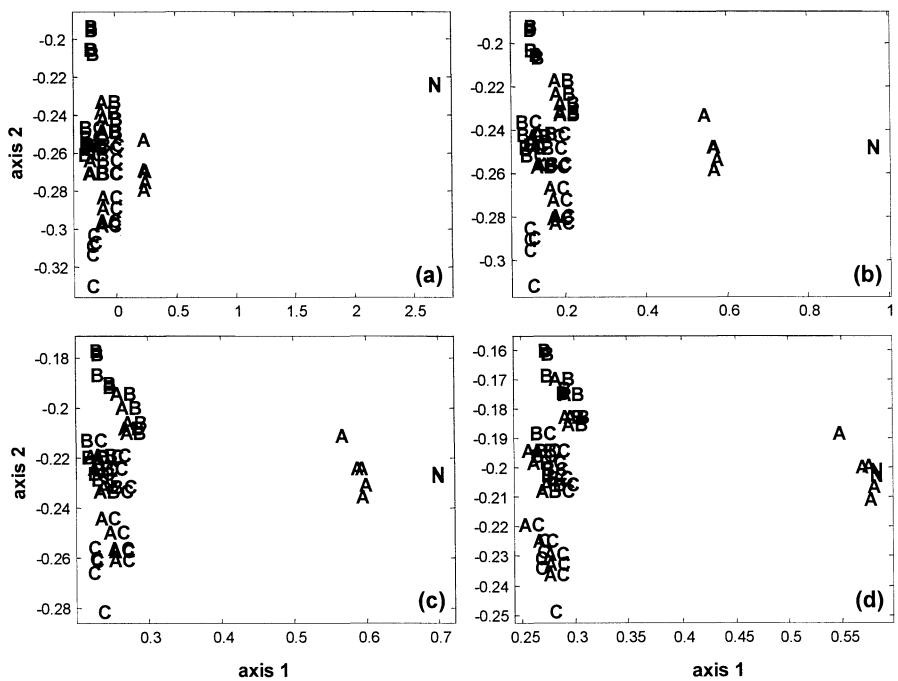

Fig. 11. Adaptation to odor A as a function of the adaptation parameter: $\eta_A = 0.05$ (a), $\eta_A = 0.35$ (b), $\eta_A = 0.65$ (c) and $\eta_A = 0.95$s (d).

5. Conclusions and Future Work

In this article we have presented two pattern recognition algorithms that mimic the effect of chemosensory adaptation on odor mixtures. The first algorithm builds a committee machine of linear discriminant functions that operate on different features subsets (or

sensor bundles) of the overall sensory input. The relative selectivity of these functions determines a set of weighting coefficients for an ensemble average, which serves as an indicator variable for each odor. An inhibitory term is included to reduce the contribution of the different sensor bundles, allowing the system to lower its sensitivity to previously detected odors. The algorithm has been evaluated on a dataset of two organic solvents and their 50/50 mixture using an array of four temperature-modulated metal-oxide gas sensors. This algorithm is best suited for mixture patterns that have a sufficient degree of complementarity.

To address the collinearity of metal-oxide gas sensors, we have presented an alternative algorithm based on Fisher's class separability criteria. The algorithm finds a low-dimensional projection that preserves an a-priori topology of odor mixtures. This topology-preserving mapping serves as the backbone for chemosensory adaptation, which is achieved by redefining the topological relationships between odors according to a desired adaptation scenario. A regularization mechanism has also been proposed to simulate different degrees of chemosensory adaptation. This topology-preserving mapping has been validated on an experimental database of binary and ternary mixtures.

Chemosensory adaptation is used in biological olfactory systems to remove constant, non-informative inputs, allowing the organism to retain its ability to detect new and potentially harmful chemical stimuli. Similarly, the adaptation algorithms presented in this article may be used in electronic-nose systems to remove background stimuli (e.g., matrix effects) and enhance the selectivity of the system towards the interesting components in a given chemical detection problem. The present study has focused on mimicking the effects of adaptation in odor mixtures, as reported in the olfaction and biological cybernetics literature [3, 4]. Additional work is being pursued to incorporate other important adaptation phenomena, such as increases in odor thresholds and cross-adaptation [25].

6. Acknowledgments

This material is based upon work supported by the National Science Foundation under CAREER Grant No. 9984426.

7. References

[1] J. W. Gardner and P. N. Bartlett, *Electronic Noses, Principles and Applications*, Oxford University Press, Oxford, UK (1999).

[2] H. T. Lawless, *Olfactory Psychophysics*, Tasting and Smelling: Handbook of Perception and Cognition 2nd ed., eds. G. K. Beauchamp and L. Bartoshuk, Academic Press, San Diego (1997) 125-175.

[3] R. A. de Wijk, *Temporal Factors in Human Olfactory perception*, Ph.D. Thesis, University of Utrecht, The Netherlands (1989).

[4] Z. Li and J. Hertz, *Odor recognition and segmentation by a model olfactory bulb and cortex*, Network: Computation in Neural Systems **11** (2000) 83-102.

[5] G. M. Shepherd, *The synaptic organization of the brain, 4th ed.*, Oxford University Press, Oxford, UK (1998).

[6] T. C. Pearce, *Computational parallels between the biological olfactory pathway and its analogue 'The Electronic Nose': Part I. Biological olfaction*, BioSystems **41**(1) (1997) 43-67.

[7] L. B. Buck and R. Axel, *A novel multigene family may encode odorant receptors: a molecular basis for odor recognition*, Cell **65** (1991) 175-187.

[8] K. J. Ressler, S. L. Sullivan and L. B. Buck, *Information coding in the olfactory system: evidence for a stereotyped and highly organized epitope map in the olfactory bulb*, Cell **79** (1994) 1245-1255.

[9] B. Malnic, J. Hirono, T. Sato and L. B. Buck, *Combinatorial receptor codes for odors*, Cell **96** (1999) 713-723.

[10] G. M. Shepherd, *Principles of specificity and redundancy underlying the organization of the olfactory system*, Microscopy Research and Technique **24** (1993) 106-112.

[11] W. Freeman, *Simulation of chaotic EEG patterns with a dynamic model of the olfactory system*, Biological Cybernetics **56** (1987) 139-150.

[12] Z. Li and J. J. Hopfield, *Modeling the Olfactory Bulb and its Neural Oscillatory Processing*, Biological Cybernetics **61** (1989) 379-392.

[13] R. Vassar, S. K. Chao, R. Sitcheran, J. M. Nuñez, L. B. Vosshall and R. Axel, *Topographic organization of sensor projections to the olfactory bulb*, Cell **79** (1994) 981-991.

[14] J. S. Kauer, *Coding in the olfactory system*, Neurobiology of Taste and Smell, eds. T. E. Finger and W. L. Silver, Wiley, New York (1987) 205-231.

[15] D. Schild, *Principles of Odor Coding and a Neural Network for Odor Discrimination*, Biophysical Journal **54** (1988) 1001-1011.

[16] Z. Li, *A Model of Olfactory Adaptation and Sensitivity Enhancement in the Olfactory Bulb*, Biological Cybernetics **62** (1990) 349-361.

[17] S. Haykin, *Neural Networks, A Comprehensive Foundation, 2nd ed.*, Prentice Hall, Upper Saddle River, NJ (1999).

[18] R. Gutierrez-Osuna, H. T. Nagle, B. Kermani and S. S. Schiffman, *Signal Conditioning and Pre-processing*, Handbook of Machine Olfaction: Electronic Nose Technology, eds. T. C. Pearce, S. S. Schiffman, H. T. Nagle and J. W. Gardner, Wiley-VCH, Weinheim, Germany (2002).

[19] M. J. Madou and S. R. Morrison, *Chemical Sensing with Solid State Devices*, Academic Press, Boston (1989).

[20] A. P. Lee and B. J. Reedy, *Temperature modulation in semiconductor gas sensing*, Sensors and Actuators B **60** (1999) 35-42.

[21] R. Gutierrez-Osuna, S. Korah and A. Perera, *Multi-Frequency Temperature Modulation for Metal-Oxide Gas Sensors*, Proc. 8th International Symposium on Olfaction and the Electronic Nose, Washington, DC (March 2001) 212-218.

[22] S. Nakata, E. Ozaki and N. Ojima, *Gas Sensing Based on the Dynamic Nonlinear Responses of a Semiconductor Gas Sensor: Dependence on the Range and Frequency of a Cyclic Temperature Change*, Analytica Chimica Acta **361** (1998) 93-100.

[23] Figaro, *General Information for TGS Sensors*, Figaro Engineering, Inc., Osaka, Japan (1996).

[24] R. O. Duda, P. E. Hart and D. G. Stork, *Pattern Classification, 2nd ed.*, Wiley, New York (2000).

[25] J. E. Cometto-Muñiz and W. S. Cain, *Olfactory Adaptation*, Handbook of Olfaction and Gustation, ed. R. L. Doty, Marcel Dekker, New York (1995) 257-281.